Sub-Micron Spectromicroscopy of UO_2 Aged Under High Humidity Conditions

Alex S. Ditter,[1] Joseph I. Pacold,[1] Zurong Dai,[2] M. Lee Davisson,[2] David Vine,[3] Scott B. Donald,[2] Brandon W. Chung,[2] and David K. Shuh[1,a]

[1]Lawrence Berkeley National Laboratory, Chemical Sciences Division, Berkeley, CA 94720
[2]Lawrence Livermore National Laboratory, Livermore, CA 94550
[3]Lawrence Berkeley National Laboratory, Advanced Light Source, Berkeley, CA 94720

[a)] Electronic mail: DKShuh@lbl.gov

The oxidation of uranium dioxide is a complicated process, depending on factors including humidity, temperature and microstructure. To further determine the characteristics of this process, UO_2 particles were allowed to age and agglomerate under 98% relative humidity at room temperature for 378 days. A focused ion beam (FIB) section of this agglomeration was then measured at the O K-edge, U N_5-edge, and C K-edge at the scanning transmission x-ray microscope (STXM) at the Advanced Light Source (ALS). O K-edge and U N_5-edge x–ray absorption measurements allowed for the elemental and chemical species mapping of the agglomerates and indicated the formation of schoepite at the sub-micron scale in specific locations. Non-negative matrix factorization (NMF) was employed to elucidate the main components at the O K-edge which were a uranyl (schoepite) formed primarily at the interface of the sample with the controlled atmosphere, a UO_2-like bulk component present in the majority of the sample, and an oxygen species present at the surface of the FIB section which is likely adsorbed water. STXM spectromicroscopy measurements at the U N_5-edge measurements also confirmed the location of oxidized uranium. This analysis is a valuable insight into the formation of schoepite on UO_2 and shows the sensitivity to and utility of STXM spectromicroscopy for uranium speciation.

I. INTRODUCTION

The oxidation of uranium dioxide is a complicated process, depending greatly on factors including humidity, temperature, microstructure, and dopants.[1-3] When stored in dry, room temperature conditions, UO_2 will quickly oxidize to form a thin layer of U_3O_7 or U_4O_9 at the surface by the incorporation of excess oxygen in octahedral holes in the fluorite lattice structure,[4-6] and will continue to oxidize the bulk of the material at a reduced rate through a diffusion controlled process.[7] In the presence of water, the higher valence uranium oxides are formed as schoepite or metaschoepite, possibly through a dissolution-precipitation process.[8,9] Studies on UO_2 powders aged under humid conditions has shown that water is a more effective oxidizer at low temperatures, but oxygen becomes more effective at higher temperatures.[10] Because this oxidation happens primarily at the surface of the sample, microstructure and surface area are highly important, key characteristics in this process.

Oxidation of UO_2 is an active area of study resulting from its technological ramifications. One key application is nuclear forensics and safeguards, where a variety of information taken from a sample of interest can be used to inform on its origin and history.[11-13] Understanding oxidation under humid conditions could allow for chemical analysis of a sample to yield information on how a sample was stored or processed.[14,15] This together with other information like isotopic abundance and morphology may help to further inform questions of recent provenance.[16] In addition to forensics applications, nuclear fuel is predominantly UO_2, and so the oxidation and resulting volume expansion of this material is critically important to designing

fuels, as well as having implications for waste storage.[17-20] Uranium oxidation is also a primary factor in understanding how uranium interacts with the environment and biological systems.[21-24]

Spectromicroscopy using a soft x-ray scanning transmission x-ray microscope (STXM) has the potential to yield a wealth of information on the oxidation and hydration of UO_2. Oxygen K-edge x-ray absorption near-edge structure (XANES) spectroscopy has been shown to be a highly sensitive tool for speciation of uranium beyond simple oxidation state determination.[25-27] A unique ability of the STXM is to focus to a spot size as small as tens of nm, allowing for fine resolution mapping of chemical species in a sample.[28-31] The uranium $N_{4,5}$-edge unlike the O K-edge, has only moderate sensitivity to uranium oxidation and contains limited chemical information,[32] whereas the carbon K-edge could yield difficult to obtain information about the nature of carbon in specific materials.

Because of the short penetration depth of soft x-rays,[33] STXM requires a thin sample, necessitating the use of a focused ion beam (FIB) to create slices which are 100-200 nm thick. STXM measurements of FIB sections have been performed before to great success,[34-41] including recent work to determine the uranium chemistry in spent nuclear fuel.[42] Given the radioactive and hazardous nature of actinide samples, the FIB sample is also ideal in that the amount of uranium is so small that specialized radiological containment is not necessary.

II. EXPERIMENTAL

A. Sample Preparation

A 10 g sample of loose powdered stoichiometric UO_2 was exposed to 760 Torr of atmospheric gas held at 98% relative humidity at room temperature for 378 days. Characterization by XRD and XPS of the powder showed that it was UO_2 prior to aging.[9] The relative humidity of the sample was controlled by placing an inorganic salt slurry of K_2SO_4 into a

vacuum desiccator, which was then allowed to equilibrate to a fixed value inside the vessel and monitored with an internal hygrometer. An aliquot of the sample was then dispensed in room air and loaded in a HEPA-filtered hood onto a carbon sticky tape mounted on a SEM stub. A FIB cut was performed in a FEI Nova600i Nanolab FESEM instrument with dual beam focus comprising a Ga+ liquid metal source FIB and a field emission gun SEM. This dual beam microscope is fitted with an Omniprobe in-situ micromanipulator and an Ascend Instruments Extreme Access (AIEA) extraction system. The material was examined by SEM in the FIB instrument and a representative particle was carefully chosen from which to extract the thin section. A platinum strap was applied onto the top surface of section using in-situ deposition induced by electron beam (e-Pt coating) and ion beam (i-Pt coating) to protect the surface structure free from bombardment damage during FIB cutting. The Pt source is $(CH_3)_3Pt(CpCH_3)$ which is first deposited as a thin carbon-rich Pt-C layer by the electron beam, and then in a much thicker Pt layer by the Ga+ ion beam.The lifted FIB section was attached to a TEM grid, which was then transferred to LBNL for STXM measurement. In total, the FIB sectioning process took approximately 8 hours.

B. STXM Measurements

The TEM grid containing the sample was affixed to an aluminum plate and loaded into the Advanced Light Source (ALS) STXM at beamline 11.0.2.[43] The chamber was evacuated then backfilled with He. STXM measurements were taken under normal operating conditions (500 mA beam current in top off mode, 1.9 GeV). The sample was rastered across the beam to generate an image of the sample. Images were taken at many energies for each edge to generate a stack. This stack then contains an x-ray absorption spectrum at each pixel of the image, which can be averaged for improved statistics or analyzed with other techniques. Measurements were

taken between 510 eV and 570 eV at the O K-edge, 710 eV and 805 eV at the U $N_{4,5}$-edge, and 275 eV and 310 eV at the C K-edge. The measurements of these spectra took approximately 1.3 hours, 1.6 hours, and 0.7 hours respectively. The FIB section was examined for a total of 8 hours in the STXM.

C. Data Processing

Data was processed using aXis2000[44] to align images and define regions of each stack to use for normalization. For each stack, a region outside the area of the sample was selected. The x-ray signal in this region was used to calculate the sample absorbance at each pixel of the images in the stack. Finally, the absorbance images were combined to generate absorption spectra with spatial resolution across the sample. Spectra were collected by selecting areas of each stack and averaging. Data at the O K-edge and U $N_{4,5}$-edges was further analyzed using non-negative matrix factorization (NMF), a technique which for STXM measurements allows for the extraction of meaningful principal components.[45,46] The specific implementation here which is well suited for STXM data has been described in previous work.[42]

The number of components used in this analysis was constrained to be three components at the O K-edge and two at the U $N_{4,5}$-edges. For the U edge, a larger number of components did not meaningfully improve fit quality. At the O K-edge, three components capture most of the variation in the data. The four-component analysis can provide a more accurate fit to the data but is unreliable in its convergence. This analysis is discussed in further detail in the SI.[47] At the U $N_{4,5}$-edges, the data was truncated to remove higher energies (including all of the U N_4 edge) due to a loss of reliable STXM focus as energy was increased. This loss of focus introduces considerable distortions in the data which makes interpreting the NMF results unintelligible if data from the U N_4-edge are included.

A high-resolution, full STXM chemical map of the entire sample is time prohibitive, so a chemical map of the entire FIB section was carried out by taking two images, one present at the schoepite peak of 531 eV, and one present at the UO_2 peak of 533 eV. The difference of these two images is used to create a false color map of the schoepite and bulk species over the entire sample. Data processing, which benefitted from the earlier NMF implementation took about 40 hours.

III. RESULTS AND DISCUSSION

A. Oxygen K-edge Measurements

Figure 1 shows a normal contrast image of the FIB section measured at 531.5 eV. The platinum FIB support and copper TEM grid are labelled along with the area that the STXM stacks for the O K-edge, U N_5-edge, and C K-edge were measured. Platinum was deposited at the surface of the sample, following the deposition of a thin carbon-rich layer, before sectioning, so the area exposed to the humid atmosphere is directly next to these two layers. The STXM stack was chosen to include both the main, upper interface of the sample with air (now bordering Pt) and largely unexposed areas of the bulk sample while still including regions without sample to normalize to.

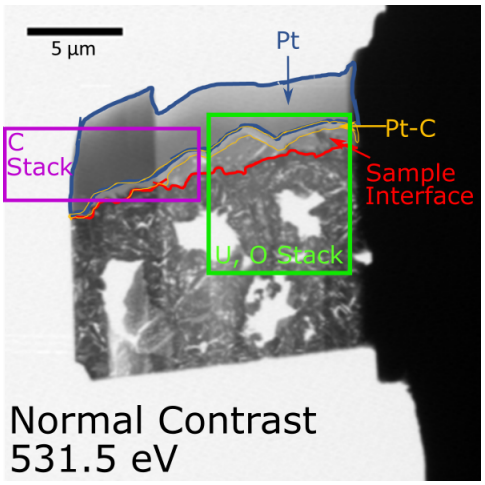

FIG. 1. Normal contrast image of the FIB section measured at 531.5 eV. The Pt (blue) and Pt-C (orange) deposition layers are labelled on the image. The main interface of the sample with the air is just below these layers, labelled in red. The rectangles define the area of the sample selected for the uranium, oxygen (green) and carbon (purple) STXM stacks that are detailed in Fig. 2, 4, and 6 (green), and 7 (purple).

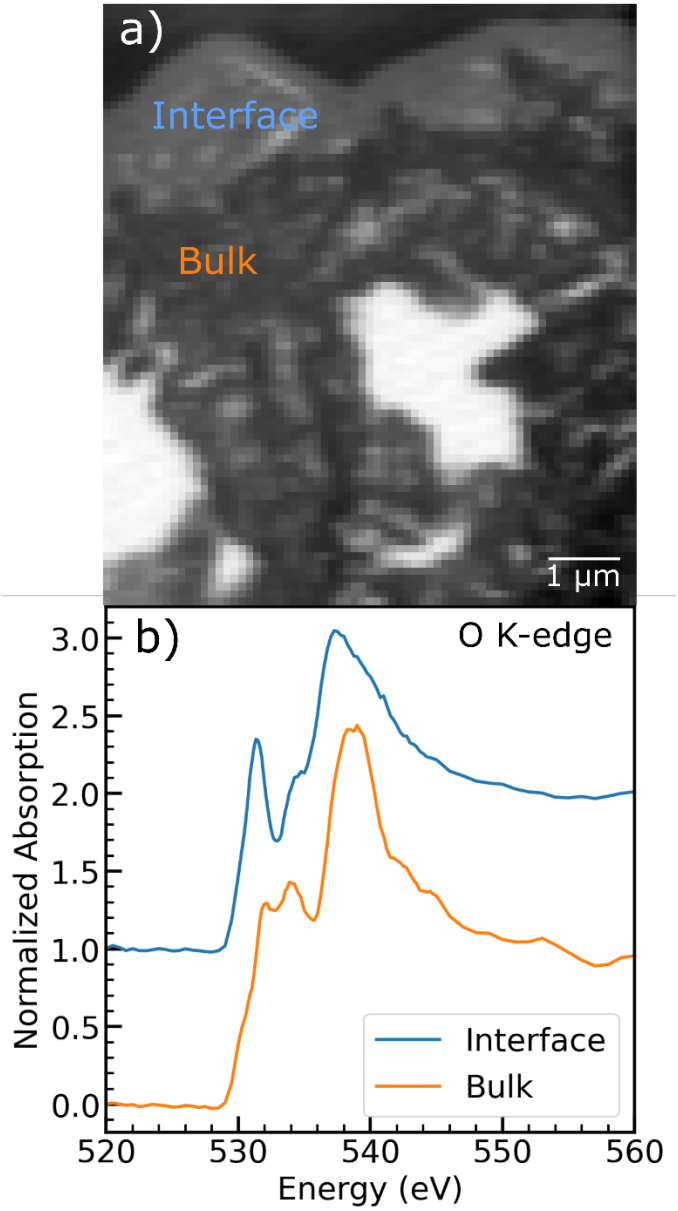

FIG. 2. a) Single image (530 eV) of stack (derived from the green area of Fig. 1). The slightly lighter area near the top is the interface of the sample with the air (before Pt deposition) and the bulk is the darker area below this. b) Average spectra taken in these two areas of this stack.

Figure 2a shows a single normal contrast image of this stack measured at 530 eV. The lighter region towards the top of the image is the interface of the sample with the controlled atmosphere (before Pt deposition) and the darker region is denoted as the bulk. Spectra averaged over these two regions are shown in Fig. 2b. The interface region shows the typical transitions

present in uranyl and uranyl bearing minerals, and the bulk region looks similar to UO_2, but with the presence of some oxidation. In particular, the peak at 531 eV is a transition into a uranyl π-antibonding orbital, and its presence in the bulk region indicates that the selected bulk region consists of UO_2 and a contribution from a higher oxide (likely schoepite or intermediates at the interface) in domains that cannot be resolved by STXM.

Inhomogeneous specimens, similar to the one that is the focus of this study, are amenable to analyses like NMF which isolate the key components of the sample. NMF separates the stack obtained by STXM spectromicroscopy into component spectra and obtains the spatial distribution of these components. Figure 3 shows the three components identified by NMF analysis. These components capture the majority of the variation across the sample, but a higher-component can provide a better fit to the data, such as the four-component fit discussed in the Supplemental Information.[47] However, the higher component fits do not consistently reproduce the same components, and so the discussion here is limited to the three component fit while acknowledging that this analysis, while capturing the main features of the O K-edge data, will miss some minor components.

The first component is attributed to the bulk component because it makes up the bulk of the sample. Furthermore, comparisons with prior measurements indicate that this spectrum is largely consistent with UO_2 with two main peaks at 532-534 eV and 539 eV. This is also consistent with other studies.[14,26,48-50] The minor peak at 530 eV is an exception to this agreement and likely is an artifact of the NMF analysis. Because NMF will yield the same results under a linear combination of components, the local minimum at 531 eV in this component indicates that some addition of the interfacial component, which has a peak there, could bring the bulk component more in line with the reference spectrum. When considering a NMF fit using a higher

number of components, a similar component to this bulk component is sometimes obtained without this initial peak, which again indicates that the three-component analysis is not fully capturing the variation in the O K-edge data and other minor oxygen species exist in this sample.[47]

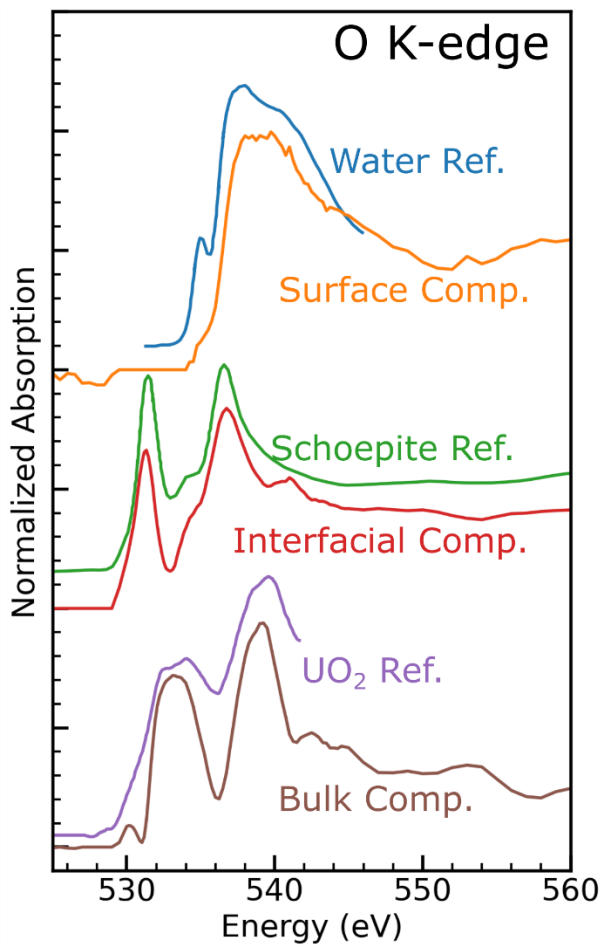

FIG. 3. Components determined by NMF analysis at the O K-edge. The bulk component (brown) is similar to UO_2 spectra previously measured (purple),[26] and the schoepite component (red) is similar to schoepite previously measured (green).[25] The surface component (orange) is present throughout the sample including on the platinum support and is similar to, but not exactly the same as the spectrum of liquid water (blue).

The second component is labelled the interfacial component as it is primarily located near the upper interface of the specimen and the controlled atmosphere prior to FIB sectioning. This

component is a uranyl phase of uranium, evidenced by the three main features of the sharp peak at 531 eV, the shoulder at 534 eV and the second main peak at 535 eV. These three features are assigned to transitions to the π^*_u, σ^*_u, and π^*_g antibonding orbitals of the central U=O bond respectively.[51] The relative strength of the σ^*_u transition is a fairly unique aspect of the oxyhydroxides measured in Ward *et al.* when compared to other possible uranyl spectra. This spectrum is also clearly distinct from UO_3 which has a lower energy first peak and broader second peak.[26,52] The main difference between this spectrum and the one measured by Ward et al. is that the first π^*_u transition is slightly less intense in the schoepite component measured here. Other minerals measured in Ward et al. have a similarly reduced relative intensity in this peak and that is attributed to the distortion of the U=O bond from other atoms like Si. In this case, the slightly reduced peak intensity could be due to the formation of amorphous rather than crystalline schoepite, slight dehydration of the schoepite, or contributions from an intermediate oxide. It could also be that this is dehydrated schoepite, which forms under high humidity conditions and could have slightly different peak intensities than schoepite.[53-55]

Finally, the third component is labelled the surface component as it forms and is found over the entirety of the sample, including the platinum coating. Because platinum is largely unreactive, this is thought to be a surface layer which has been adsorbed on the sample after FIB sectioning. The spectrum is similar and resembles, but is not exactly the same as water, which is one possibility for this surface constituent, though other possibilities cannot be fully excluded. The main difference between the surface component obtained here and a liquid water spectrum it is that the pre-edge feature at 535 eV is absent in the surface component spectrum. This feature has been shown to be dependent on the hydrogen bonds formed in liquid water, so if this water is primarily adsorbed to the surface of the FIB section it is not surprising that the intensity of this

feature would change for the surface component which has substantial interactions with the surface of the sample. An extensive investigation of potential oxygen compounds adsorbed to the surface is not presented here as the surface of the FIB section is not the main focus of this analysis.

Figure 4 shows the spatial locations of the three components from the specimen. As mentioned earlier the surface component is present throughout the sample, including the platinum region (top). The bulk component and schoepite components are largely exclusive of each other, with the bulk making up the majority of the sample, and the schoepite is concentrated at the interface and grains. However, some schoepite is present throughout the bulk of the sample, indicating that there are small regions of schoepite in at the sample bulk interface which are too small to resolved distinctly by STXM. This is expected, given the spectrum obtained by averaging over a bulk area in Fig. 2 had some characteristics of uranyl, namely the peak at 531 eV. Because this is a thin slice through a three-dimensional agglomeration, there are regions of primarily interfacial component that do not appear near a void in the sample (i.e., the long inclusion to the left of the central void in Fig. 3.), that may in fact have been near a void in three-dimensional space prior to FIB sectioning. The schoepite is concentrated both at the interface of the sample (near the platinum) and in inclusions in the bulk of the sample.

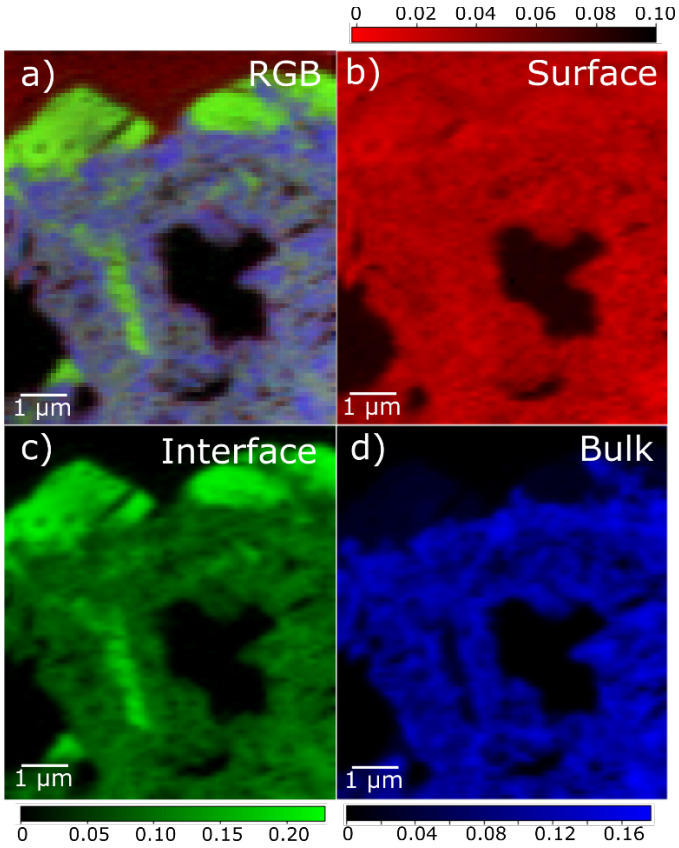

FIG. 4. a) RGB image of the three components identified by NMF analysis. These components are the b) surface component, c) interface component, and d) bulk component. The scale at the bottom is optical density above the edge for each component (proportional to oxygen quantity in each phase).

Figure 5 shows a chemical map of the entire FIB section. Blue areas indicate schoepite concentration and red areas are mainly bulk oxide. This indicates that there are several volumes where schoepite is present in the interior of the sample since these regions are near voids exposed to the controlled atmosphere, later exposed by FIB sectioning.

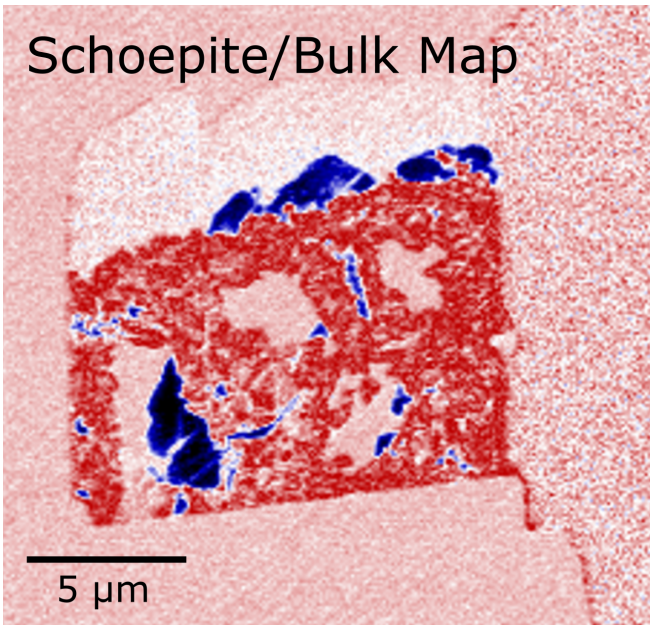

FIG. 5. False-color chemical map of entire FIB section generated by subtracting two images taken at different energies. Blue areas indicate higher schoepite content and red areas indicate bulk UO_2-like uranium.

B. U N_5-edge

Results from the U N_5-edge are given in Fig. 6 and Fig. 6a shows the two components. The first is labeled bulk as it is located throughout the bulk of the sample. The other is labeled schoepite because it is located in the same areas of the sample where schoepite was identified. The peak of the schoepite component is higher in energy than the bulk component by approximately 1.8 eV, which is similar to prior measurements at this edge.[56,57] Because STXM focus was lost approaching the U N_4-edge, a branching ratio analysis is not possible. The spatial maps of these components are shown in Fig. 6b and 6c. The locations of these components match up very well with the bulk and schoepite components measured at the O K-edge. This is an important confirmation of the results from the oxygen K-edge, but this also shows that the U N-edges can be used for oxidation state mapping, which can be very useful for compounds where

the ligand edge is either not easily measurable or ambiguous such as in solid solutions like mixed oxide fuels.

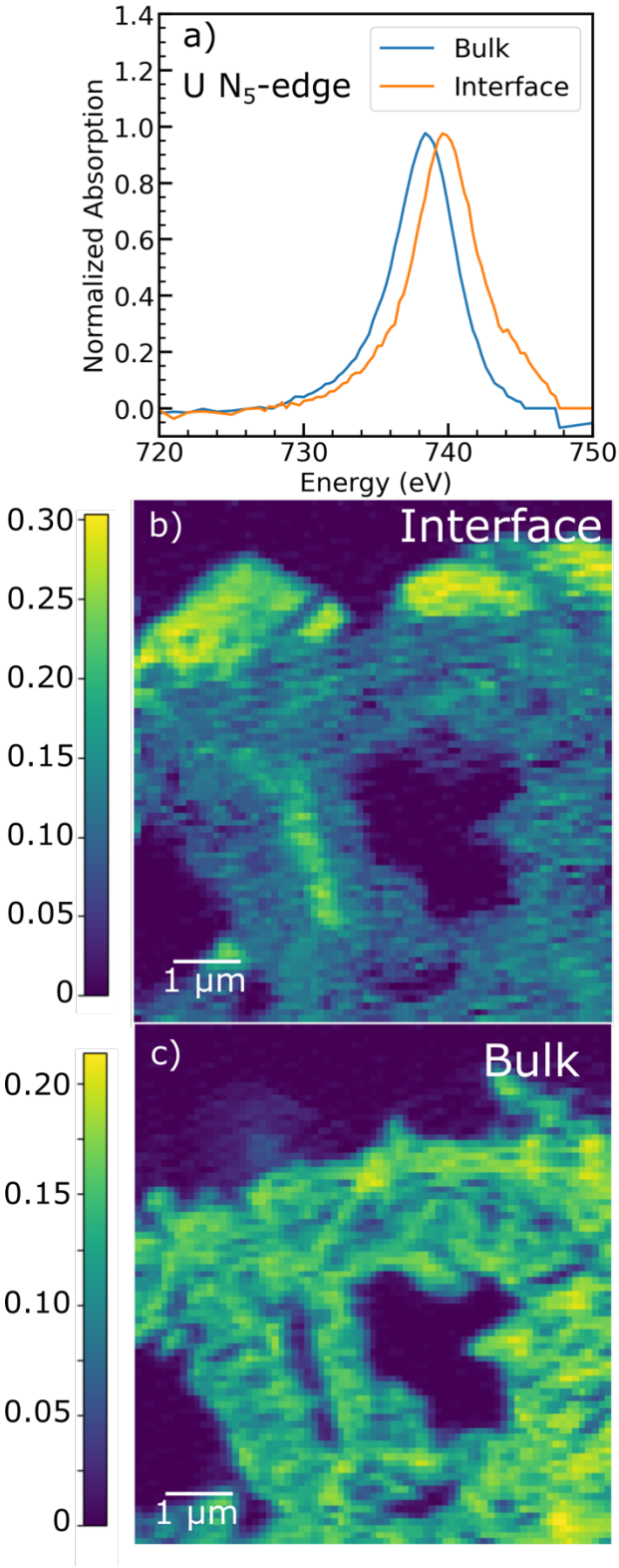

FIG. 6. NMF fit results on a U N_5-edge map collected in the same region as the O K-edge stack (area given by the green rectangle in Fig. 1). a) Components determined by NMF fitting at the U N_5-edge. Spatial map of the interfacial (b) and bulk (c) components which matches well with O K-edge components.

C. C K-edge

Figure 7a shows the area of a stack taken at the C K-edge (near the top-right of the sample). Fig. 7b is the C K-edge spectrum collected over the corner of the stack in which sample material was present. Carbon is a challenging edge to measure due to its low photon energy and the tendency of carbon to build up on a sample during measurement. However, the presence of carbon can be a vital piece of compositional information and an important clue to the history of a sample. Maps of carbon could be particularly important, highlighting areas of interest on a sample, and STXM spectromicroscopy is one of the few techniques capable of conducting a detailed chemical analysis of carbon at this scale.

The predominant feature of this carbon spectrum is the main peak at approximately 285 eV. This is similar to graphite which has a strong 1s to π* antibonding orbital transition at this energy.[58,59] Graphite also has a distinctive 1s-σ* antibonding orbital at approximately 290 eV, but in the case of amorphous carbon, this transition is broadened and less distinct, which is similar to the carbon spectrum observed here.[60] This is not the only possibility, as this π* antibonding orbital transition is present in the spectra of many hydrocarbons as well, which have a wide variation to their spectra.[61,62] The deposition of carbon during FIB sectioning is well known and both hydrocarbons and amorphous carbon are species which have been observed in this context in the past.[63]

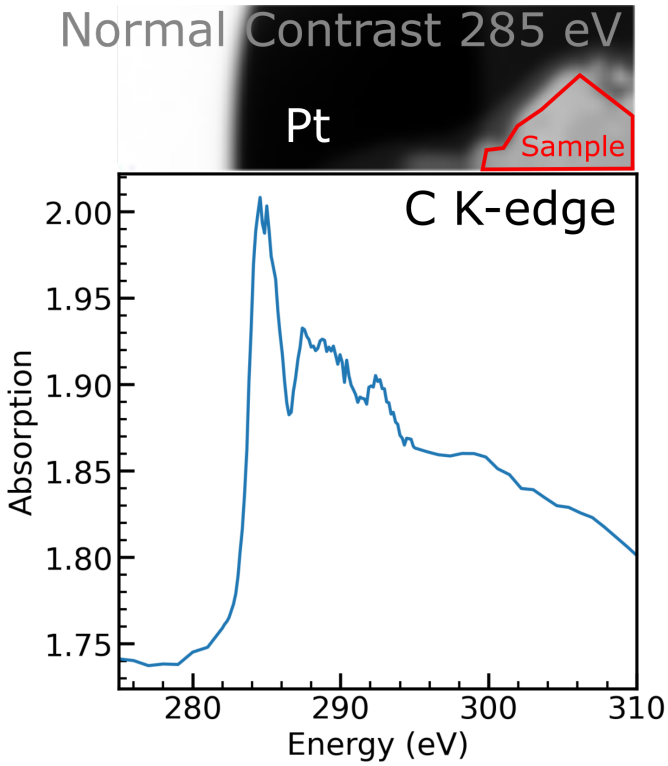

FIG. 7. a) Normal contrast image showing the location of the C K-edge stack on the sample (see Fig. 1 for context). At left is the Pt and carbon-rich Pt deposition layers (dark), whereas the light part of the image consists of the sample. (b) C K-edge spectrum averaged over the red region of the stack labelled "sample" in a).

IV. SUMMARY AND CONCLUSIONS

UO_2 was aged for 378 days under high humidity conditions and examined using STXM spectromicroscopy to understand how the UO_2 changes under these conditions. An interfacial, amorphous schoepite and bulk UO_2 phase are identified from NMF with the possibility of the schoepite being slightly dehydrated. The schoepite is located in large areas at the interfaces of the sample (particularly the upper interface), but also in smaller interfacial regions throughout the sample. This is confirmed by U N_5-edge measurements which are consistent with the O K-edge results and show utility for future oxidation state measurements at this edge. Non-negative

matrix factorization was shown to be particularly valuable in discerning the different phases of uranium in the sample and mapping these spatially. Carbon K-edge spectromicroscopy was also demonstrated, showing the utility of this approach for characterizing carbon and carbon speciation in specimens prepared by FIB.

The oxygen K-edge has a unique sensitivity for uranium oxide speciation that is difficult to achieve with other techniques. In particular, full chemical speciation of amorphous samples is particularly difficult using electron microscopy diffraction or x-ray diffraction. The ability to identify and precisely determine the location of schoepite is an invaluable piece of information within in a forensics context that yields insight into the provenance of the specimen. Coupling STXM spectromicroscopy with FIB sectioning allows for soft x-ray measurements which are sensitive to both the bulk and interface of a sample with resolution better than 50 nm. Since only a small amount of material is required, this technique could be used with even highly radioactive materials. Moving forward, the combination of STXM and FIB sectioning technique has shown to be a valuable tool for the study of nuclear forensics, safeguards, advanced fuels, and environmental specimens.

ACKNOWLEDGMENTS

This work was performed under the auspices of the U.S. Department of Energy (DOE) by Lawrence Berkeley National Laboratory (LBNL) (AD, JIP, DKS) under Contract Number DE-AC02-05CH11231 and Lawrence Livermore National Laboratory (LLNL) under Contract DE-AC52-07NA27344. The work was funded by the Office of Defense Nuclear Nonproliferation Research and Development within the DOE National Nuclear Security Administration (NNSA) under the competitively awarded projects LL15-U_Surface_Oxidation-NDD3B, LL22-ML-FIBmicro-NTNF1Ba, and LB14-FY14-070NDD3. This research used resources of the Advanced

Light Source (Beamline 11.0.2.2 and DV) which is a DOE Office of Science User Facility under Contract Number DE-AC02-05CH11231. The views, opinions and findings contained within this paper are those of the authors and should not be construed as an official position, policy or decision of the DOE unless designated by other documentation. LLNL-JRNL-832881

CONFLICT OF INTEREST

The authors have no conflicts to disclose.

DATA AVAILABILITY

Data is available upon a reasonable request to the authors.

REFERENCES

[1] L. E. Thomas, R. E. Einziger, and H. C. Buchanan, J. Nucl. Mater. 201, 310 (1993). 10.1016/0022-3115(93)90187-4

[2] I. Grenthe, J. Drożdżyński, T. Fujino, E. C. Buck, T. E. Albrecht-Schmitt, and S. F. Wolf, in *The Chemistry of the Actinide and Transactinide Elements*, edited by L. R. Morss, N. M. Edelstein, and J. Fuger (Springer Netherlands, Dordrecht, 2006), pp. 253. 10.1007/1-4020-3598-5_5

[3] R. J. McEachern and P. Taylor, J. Nucl. Mater. 254, 87 (1998). 10.1016/S0022-3115(97)00343-7

[4] G. Leinders, R. Delville, J. Pakarinen, T. Cardinaels, K. Binnemans, and M. Verwerft, Inorg. Chem. 55, 9923 (2016). 10.1021/acs.inorgchem.6b01941

[5] G. Leinders, R. Bes, K. O. Kvashnina, and M. Verwerft, Inorg. Chem. 59, 4576 (2020). 10.1021/acs.inorgchem.9b03702

[6] J. M. Elorrieta, L. J. Bonales, N. Rodríguez-Villagra, V. G. Baonza, and J. Cobos, Phys. Chem. Chem. Phys. 18, 28209 (2016). 10.1039/C6CP03800J

[7] H. R. Hoekstra, A. Santoro, and S. Siegel, J. Inorg. Nucl. Chem. 18, 166 (1961). 10.1016/0022-1902(61)80384-9

[8] R. J. Finch and R. C. Ewing, J. Nucl. Mater. 190, 133 (1992). 10.1016/0022-3115(92)90083-W

[9] S. B. Donald, Z. R. Dai, M. L. Davisson, J. R. Jeffries, and A. J. Nelson, J. Nucl. Mater. 487, 105 (2017). 10.1016/j.jnucmat.2017.02.016

[10] S. B. Donald, M. L. Davisson, Z. Dai, S. K. Roberts, and A. J. Nelson, J. Nucl. Mater. 496, 353 (2017). 10.1016/j.jnucmat.2017.10.014

[11] K. J. Moody, P. M. Grant, I. D. Hutcheon, and Y. Varoufakis, *Nuclear Forensic Analysis* (CRC Press, Boca Raton, 2014), 10.1201/b17863

[12] I. D. Hutcheon, M. J. Kristo, and K. B. Knight, in *Uranium: Cradle to Grave* (Mineralogical Association of Canada, Quebec, Quebec, 2013).

[13] M. J. Kristo and S. J. Tumey, Nucl. Instrum. Meth. B. 294, 656 (2013). 10.1016/j.nimb.2012.07.047

[14] J. I. Pacold, A. B. Altman, K. B. Knight, K. S. Holliday, M. J. Kristo, S. G. Minasian, T. Tyliszczak, C. H. Booth, and D. K. Shuh, Analyst 143, 1349 (2018). 10.1039/C7AN01838J

[15] J. I. Pacold, A. B. Altman, S. B. Donald, Z. Dai, M. L. Davisson, K. S. Holliday, K. B. Knight, M. J. Kristo, S. G. Minasian, A. J. Nelson, T. Tyliszczak, C. H. Booth, and D. K. Shuh, Final Report on Small Particle Speciation for Forensics Analysis by Soft X-ray Scanning Transmission X-ray Microscopy, 2016. US DOE Report LLNL-TR-704343. 10.2172/1358309

[16] E. J. Oerter, M. Singleton, Z. Dai, S. Donald, M. Thaw, and M. L. Davisson, Talanta 226, 122096 (2021). 10.1016/j.talanta.2021.122096

[17] R. C. Ewing, Nat. Mater. 14, 252 (2015). 10.1038/nmat4226

[18] I. J. Hastings, A. D. Smith, P. J. Fehrenbach, and T. J. Carter, J. Nucl. Mater. 139, 106 (1986). 10.1016/0022-3115(86)90028-0

[19] M. Tonks, D. Andersson, R. Devanathan, R. Dubourg, A. El-Azab, M. Freyss, F. Iglesias, K. Kulacsy, G. Pastore, S. R. Phillpot, and M. Welland, J. Nucl. Mater. 504, 300 (2018). 10.1016/j.jnucmat.2018.03.016

[20] J. M. Haschke, J. Alloy. Compd. 278, 149 (1998). 10.1016/S0925-8388(98)00639-2

[21] D. Langmuir, Geochim. Cosmochim. Acta 42, 547 (1978). 10.1016/0016-7037(78)90001-7

[22] David M. Taylor and Sarah K. Taylor, Rev. Environ. Health. 12, 147 (1997). 10.1515/REVEH.1997.12.3.147

[23] S. A. Cumberland, G. Douglas, K. Grice, and J. W. Moreau, Earth-Sci. Rev. 159, 160 (2016). 10.1016/j.earscirev.2016.05.010

[24] M. P. Elless and S. Y. Lee, Water Air Soil Poll. 107, 147 (1998). 10.1023/A:1004982515941

[25] J. D. Ward, M. Bowden, C. T. Resch, S. Smith, B. K. McNamara, E. C. Buck, G. C. Eiden, and A. M. Duffin, Geostand. Geoanal. Res. 40, 135 (2016). 10.1111/j.1751-908X.2015.00337.x

[26] S. D. Conradson, T. Durakiewicz, F. J. Espinosa-Faller, Y. Q. An, D. A. Andersson, A. R. Bishop, K. S. Boland, J. A. Bradley, D. D. Byler, D. L. Clark, D. R. Conradson, L. L. Conradson, A. L. Costello, N. J. Hess, G. H. Lander, A. Llobet, M. B. Martucci, J. Mustre de Leon, D. Nordlund, J. S. Lezama-Pacheco, T. E. Proffen, G. Rodriguez, D. E. Schwarz, G. T. Seidler, A. J. Taylor, S. A. Trugman, T. A. Tyson, and J. A. Valdez, Phys. Rev. B. 88, 115135 (2013). 10.1103/PhysRevB.88.115135

[27] F. Frati, M. O. J. Y. Hunault, and F. M. F. de Groot, Chem. Rev. 120, 4056 (2020). 10.1021/acs.chemrev.9b00439

[28] A. P. Hitchcock, J. Electron. Spectrosc. 200, 49 (2015). 10.1016/j.elspec.2015.05.013

[29] A. Sakdinawat and D. Attwood, Nat. Photonics. 4, 840 (2010). 10.1038/nphoton.2010.267

[30] C. Jacobsen, S. Williams, E. Anderson, M. T. Browne, C. J. Buckley, D. Kern, J. Kirz, M. Rivers, and X. Zhang, Opt. Commun. 86, 351 (1991). 10.1016/0030-4018(91)90016-7

[31] Jacobsen, Wirick, Flynn, and Zimba, J. Microsc. 197, 173 (2000). 10.1046/j.1365-2818.2000.00640.x

[32] J. G. Tobin, J. Electron. Spectrosc. 194, 14 (2014). 10.1016/j.elspec.2014.01.020

[33] CXRO X-ray Database, cxro.lbl.gov.

[34] K. Benzerara, N. Menguy, N. R. Banerjee, T. Tyliszczak, G. E. Brown, and F. Guyot, Earth Planet. Sc. Lett. 260, 187 (2007). 10.1016/j.epsl.2007.05.029

[35] A. Michelin, E. Drouet, E. Foy, J. J. Dynes, D. Neff, and P. Dillmann, J. Anal. Atom. Spectrom. 28, 59 (2013). 10.1039/C2JA30250K

[36] S. Bernard, K. Benzerara, O. Beyssac, N. Menguy, F. Guyot, G. E. Brown, and B. Goffé, Earth Planet. Sc. Lett. 262, 257 (2007). 10.1016/j.epsl.2007.07.041

[37] S. Bernard, K. Benzerara, O. Beyssac, G. E. Brown, L. G. Stamm, and P. Duringer, Rev. Palaeobot. Palyno. 156, 248 (2009). 10.1016/j.revpalbo.2008.09.002

[38] H. Yabuta, M. Uesugi, H. Naraoka, M. Ito, A. L. D. Kilcoyne, S. A. Sandford, F. Kitajima, H. Mita, Y. Takano, T. Yada, Y. Karouji, Y. Ishibashi, T. Okada, and M. Abe, Earth Planet. Sp. 66, 156 (2014). 10.1186/s40623-014-0156-0

[39] M. Uesugi, H. Naraoka, M. Ito, H. Yabuta, F. Kitajima, Y. Takano, H. Mita, I. Ohnishi, Y. Kebukawa, T. Yada, Y. Karouji, Y. Ishibashi, T. Okada, and M. Abe, Earth Planet. Sp. 66, 102 (2014). 10.1186/1880-5981-66-102

[40] M. Ito, N. Tomioka, K. Uesugi, M. Uesugi, Y. Kodama, I. Sakurai, I. Okada, T. Ohigashi, H. Yuzawa, A. Yamaguchi, N. Imae, Y. Karouji, N. Shirai, T. Yada, and M. Abe, Earth Planet. Sp. 72, 133 (2020). 10.1186/s40623-020-01267-2

[41] L. Gu, N. Wang, X. Tang, and H. G. Changela, Scanning, 8406917 (2020). 10.1155/2020/8406917

[42] A. S. Ditter, D. E. Smiles, D. Lussier, A. B. Altman, M. Bachhav, L. He, M. W. Mara, C. Degueldre, S. G. Minasian, and D. K. Shuh, J. Synch. Rad. 29, 67 (2022). 10.1107/S1600577521012315

[43] H. Bluhm, K. Andersson, T. Araki, K. Benzerara, G. E. Brown, J. J. Dynes, S. Ghosal, M. K. Gilles, H. C. Hansen, J. C. Hemminger, A. P. Hitchcock, G. Ketteler, A. L. D. Kilcoyne, E. Kneedler, J. R. Lawrence, G. G. Leppard, J. Majzlam, B. S. Mun, S. C. B. Myneni, A. Nilsson, H. Ogasawara, D. F. Ogletree, K. Pecher, M. Salmeron, D. K. Shuh, B. Tonner, T. Tyliszczak, T. Warwick, and T. H. Yoon, J. Electron. Spectrosc. 150, 86 (2006). 10.1016/j.elspec.2005.07.005

[44] aXis2000, http://unicorn.mcmaster.ca/aXis2000.html.

[45] D. D. Lee and H. S. Seung, Nature 401, 788 (1999). 10.1038/44565

[46] R. Mak, M. Lerotic, H. Fleckenstein, S. Vogt, S. M. Wild, S. Leyffer, Y. Sheynkin, and C. Jacobsen, Faraday Discuss. 171, 357 (2014). 10.1039/C4FD00023D

[47] See supplementary material at [URL will be inserted by AIP Publishing] for a discussion of the limitations of the three-component NMF analysis and a four-component fit at the O K-edge.

[48] J. G. Tobin, A. M. Duffin, S. W. Yu, R. Qiao, W. L. Yang, C. H. Booth, and D. K. Shuh, J. Vac. Sci. Technol. A 35, 03E108 (2017). 10.1116/1.4979540

[49] F. Jollet, T. Petit, S. Gota, N. Thromat, M. Gautier-Soyer, and A. Pasturel, J. Phys.-Condens. Mat. 9, 9393 (1997). 10.1088/0953-8984/9/43/022

[50] J. D. Ward, M. Bowden, C. Tom Resch, G. C. Eiden, C. D. Pemmaraju, D. Prendergast, and A. M. Duffin, Spectrochim. Acta. B. 127, 20 (2017). 10.1016/j.sab.2016.11.008

[51] C. Fillaux, D. Guillaumont, J.-C. Berthet, R. Copping, D. K. Shuh, T. Tyliszczak, and C. D. Auwer, Phys. Chem. Chem. Phys. 12, 14253 (2010). 10.1039/C0CP00386G

[52] M. Magnuson, S. M. Butorin, L. Werme, J. Nordgren, K. E. Ivanov, J. H. Guo, and D. K. Shuh, Appl. Surf. Sci. 252, 5615 (2006). 10.1016/j.apsusc.2005.12.131

[53] P. Taylor, D. D. Wood, A. M. Duclos, and D. G. Owen, J. Nucl. Mater. 168, 70 (1989). 10.1016/0022-3115(89)90566-7

[54] P. Taylor, D. D. Wood, D. G. Owen, and G.-I. Park, J. Nucl. Mater. 183, 105 (1991). 10.1016/0022-3115(91)90477-O

[55] P. Taylor, R. J. Lemire, and D. D. Wood, Nucl. Technol. 104, 164 (1993). 10.13182/NT93-A34880

[56] J. G. Tobin, S. W. Yu, C. H. Booth, T. Tyliszczak, D. K. Shuh, G. van der Laan, D. Sokaras, D. Nordlund, T. C. Weng, and P. S. Bagus, Phys. Rev. B. 92, 035111 (2015). 10.1103/PhysRevB.92.035111

[57] H. J. Nilsson, T. Tyliszczak, R. E. Wilson, L. Werme, and D. K. Shuh, Anal. Bioanal. Chem. 383, 41 (2005). 10.1007/s00216-005-3355-5

[58] S. D. Berger, D. R. McKenzie, and P. J. Martin, Phil. Mag. Lett. 57, 285 (1988). 10.1080/09500838808214715

[59] P. A. Brühwiler, A. J. Maxwell, C. Puglia, A. Nilsson, S. Andersson, and N. Mårtensson, Phys. Rev. Lett. 74, 614 (1995). 10.1103/PhysRevLett.74.614

[60] J. Díaz, S. Anders, X. Zhou, E. J. Moler, S. A. Kellar, and Z. Hussain, Phys. Rev. B 64, 125204 (2001). 10.1103/PhysRevB.64.125204

[61] J. Stöhr, F. Sette, and A. L. Johnson, Phys. Rev. Lett. 53, 1684 (1984). 10.1103/PhysRevLett.53.1684

[62] J. L. Jordan-Sweet, C. A. Kovac, M. J. Goldberg, and J. F. Morar, J. Chem. Phys. 89, 2482 (1988). 10.1063/1.455042

[63] N. T. H. Farr, G. M. Hughes, and C. Rodenburg, Materials 14, 3034 (2021).